JCI insight

Tristetraprolin expression by keratinocytes protects against skin carcinogenesis

Assiya Assabban, … , Perry J. Blackshear, Stanislas Goriely

JCI Insight. 2021. https://doi.org/10.1172/jci.insight.140669.

Research In-Press Preview Inflammation Oncology

Graphical abstract

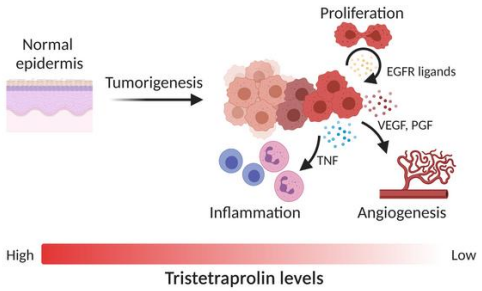

Tristetraprolin expression by keratinocytes protects against skin carcinogenesis

Assiya Assabban[1], Ingrid Dubois-Vedrenne[1*], Laurye Van Maele[1*], Rosalba Salcedo[2], Brittany Snyder[3], Lecong Zhou[4], Abdulkader Azouz[1], Bérengère de Toeuf[5], Gaëlle Lapouge[6], Caroline La[1], Maxime Melchior[1], Muriel Nguyen[1], Séverine Thomas[1], Sifan Wu[5], Wenqian Hu[7], Véronique Kruys[5], Cédric Blanpain[6], Giorgio Trinchieri[2], Cyril Gueydan[5], Perry J. Blackshear[3,8†] and Stanislas Goriely[1†]

Affiliations :

[1] Institute for Medical Immunology, Université Libre de Bruxelles, Gosselies, Belgium, ULB Center for Research in Immunology (U-CRI) and ULB Center for Cancer Research (U-CRC).

[2]Cancer and Inflammation Program, Center for Cancer Research, National Cancer Institute, National Institutes of Health, Bethesda, Maryland 20892

[3]Signal Transduction Laboratory, National Institute of Environmental Health Sciences, Research Triangle Park, North Carolina, USA, 27709

[4]Integrative Bioinformatics Support Group, National Institute of Environmental Health Sciences, Research Triangle Park, NC 27709

[5]Laboratoire de Biologie Moléculaire du Gène, Université Libre de Bruxelles, Gosselies, Belgium

[6] Laboratory of Stem Cells and Cancer, Université Libre de Bruxelles, Brussels, Belgium, WELBIO and ULB Center for Cancer Research (U-CRC).

[7]Department of Biochemistry & Molecular Biology, Mayo Clinic, Rochester, USA

[8]Departments of Medicine and Biochemistry, Duke University Medical Center, Durham, NC 27710, USA

*These authors contributed equally

†These authors contributed equally

Lead contact:

S. GORIELY, Institute for Medical Immunology, 8 rue Adrienne Bolland, B-6041

Charleroi-Gosselies, Belgium; Phone: 32-2-650-9588; Fax: 32-2-650-9563; E-mail: stgoriel@ulb.ac.be

The authors have no conflict of interest to disclose

Abstract

Cancer is caused primarily by genomic alterations resulting in deregulation of gene regulatory circuits in key growth, apoptosis or DNA repair pathways. Multiple genes associated with the initiation and development of tumors are also regulated at the level of mRNA decay, through the recruitment of RNA binding proteins to AU-rich elements (AREs) located in their 3'-untranslated regions. One of these ARE-binding proteins, tristetraprolin (TTP, encoded by *Zfp36*) is consistently dysregulated in many human malignancies. Herein, using regulated overexpression or conditional ablation in the context of chemical cutaneous carcinogenesis, we show that TTP represents a critical regulator of skin tumorigenesis. We provide evidence that TTP controls both tumor-associated inflammation and key oncogenic pathways in neoplastic epidermal cells. We identify *Areg* as a direct target of TTP in keratinocytes, and show that EGFR signaling potentially contributes to exacerbated tumor formation. Finally, single-cell RNA-Sequencing analysis indicates that *ZFP36* is downregulated in human malignant keratinocytes. We conclude that TTP expression by epidermal cells plays a major role in the control of skin tumorigenesis.

Introduction

Tumors arise when gene regulatory circuits in key growth, apoptosis or DNA repair pathways are dysregulated. Oncogenic events such as mutations in proto-oncogenes can radically affect cell physiology through downstream effects on gene expression, for example by aberrant activation of transcription factors. Gene expression pathways may also be affected by alterations in post-transcriptional mechanisms, i.e., by modulating mRNA stability and/or their translational potential. Up to 10% of mammalian mRNAs harbor AU-rich elements (AREs) in their 3' untranslated regions, allowing the recruitment of RNA-binding proteins that control their turnover and subcellular localization. One of these ARE-binding proteins is tristetraprolin (TTP, encoded by *ZFP36*). TTP targets these ARE-containing mRNAs for degradation by recruitment of deadenylase complexes. Decreased expression or function of TTP is consistently observed in many human malignancies, and multiple types of evidence now indicate that deregulation of ARE-mediated mRNA decay could represent a cardinal feature of tumor biology (1). For example, in breast tumor cell lines, miR-29a can regulate TTP expression, directly affecting epithelial polarity and metastasis (2). In hepatocellular carcinoma cell lines, hypermethylation of the *Zfp36* promoter favors tumor growth (3), while in glioma cell lines, hyperphosphorylated forms of TTP predominate, increasing VEGF and IL8 mRNA stability (4). Interestingly, *ZFP36* polymorphisms are associated with poor prognosis in breast cancer patients (5). Myc oncoprotein directly suppresses TTP expression, leading to aberrant overexpression of ARE-containing mRNAs (6). Furthermore, oncogenic Ras signaling was shown to modulate TTP activity, leading to increased PD-L1 expression, indicating that this pathway may negatively affect anti-tumoral immune responses (7).

Importantly, TTP plays a major role in the control of inflammation, which represents a cardinal feature of tumor development. In macrophages and dendritic cells, TTP controls the production of key inflammatory cytokines such as TNF, IL-1β, IL-6 and IL-23 (8–10).

Furthermore, in keratinocytes, TTP contributes to skin immune homeostasis by regulating TNF production (11). In line with these observations, TTP-deficient mice spontaneously develop a complex TNF- and IL-23-dependent inflammatory syndrome characterized by cachexia, progressive dermatitis, arthritis and myeloid hyperplasia (9,12). Herein, using a knock-in model of regulated TTP overexpression (13) and a conditional TTP deficient model (11) in the context of chemical cutaneous carcinogenesis, we show that TTP represents a critical regulator of skin tumorigenesis. We further provide evidence that TTP controls both tumor-associated inflammation and key oncogenic pathways in neoplastic epidermal cells.

Results

Regulated overexpression of endogenous TTP protects mice from cutaneous chemical carcinogenesis

Multiple lines of evidence support a major role for dysregulation of mRNA decay in cancer. However, most of the direct evidence for a role of TTP in cancer biology stems from studies using in vitro or transplantable tumor cell lines. It is clear that these models do not recapitulate the complex interactions between tumor, stromal and immune cells. In order to explore the role of TTP in early phases of tumor development, we used the classic two-step skin chemical carcinogenesis model in *Zfp36*$^{\Delta ARE}$ mice. In these mice, a 136-base instability motif in the 3′-UTR of TTP mRNA was deleted in the endogenous genetic locus, leading to enhanced, systemic TTP protein expression, and decreased susceptibility to several models of inflammatory disease (13). Consistent with previous reports (14), upon treatment with 7,12-dimethylbenz[a]anthracene (DMBA) followed by bi-weekly 12-0 tetradecanoylphorbol-13-acetate (TPA) application over the course of 10-18 weeks, all control mice developed multiple papillomas (Figure 1A). The tumor burden was strikingly reduced and delayed in the *Zfp36*$^{\Delta ARE}$ mice, with half of the animals remaining tumor-free after 20 weeks of treatment.

Upon termination of the experiment, we performed RNA-Seq on treated adjacent non-tumoral whole skin samples from both groups. We observed 1144 statistically differentially expressed genes (232 and 912 up- and down-regulated genes in *Zfp36*$^{\Delta ARE}$ mice, respectively, with a fold change>2 and FDR<0.05) (Figure 1B). As expected, *Zfp36* mRNA expression was increased by approximately 3-fold in the skin of *Zfp36*$^{\Delta ARE}$ mice (Figure 1C). Furthermore, expression of its paralogs, *Zfp36l1* and *Zfp36l2,* was largely equivalent in both groups, while the placenta- and yolk-sac specific paralog *Zfp36l3* was undetectable. We observed a strong enrichment for innate immunity, myeloid cells and inflammation-related pathways among genes that were

down-regulated in the *Zfp36*$^{\Delta ARE}$ samples, indicating that TTP overexpression restricts inflammation in these chronically stimulated skin samples (Figure 1D). This is consistent with previous results showing that *Zfp36*$^{\Delta ARE}$ mice are protected from imiquimod-induced dermatitis (13). In addition to known TTP targets (eg. *Cxcl2* or *Il23a*), many genes expressed by myeloid cells (*Cd163, CD14, Fcer1g, Csfr1, Tlrs*) were found to be decreased, suggesting decreased recruitment and activation of innate immune cells (Figure 1E). Taken together, these data indicate that increased systemic TTP expression from its endogenous locus protects mice from inflammation-induced skin carcinogenesis.

Expression of TTP by epidermal cells rather than myeloid cells plays a major role in the control of skin carcinogenesis.

In order to define in which cell types TTP was active in preventing skin carcinogenesis, we then assessed TTP protein expression in cells isolated from the skin after short-term treatment with TPA. Unfortunately, most available anti-TTP antibodies cannot be reliably used for FACS staining. To circumvent this technical problem, we used a *Zfp36-V5* epitope tagged knock-in mouse generated by CRISPR/Cas9-mediated genome editing (15). We observed consistent TTP-V5 staining in myeloid cells from acetone-treated mice that was further increased upon TPA treatment. The highest expression levels were observed in macrophages and DC subsets. In parallel, we assessed TTP-V5 expression in keratinocytes. We detected low levels after acetone treatment, but markedly increased expression after TPA treatment, reaching levels comparable to that observed in macrophages or DCs from TPA-treated skin (Figure 2A). Based on this result, we decided to evaluate the contribution of TTP expressed in these different cell types. For this purpose, we deleted *Zfp36* in myeloid cells (LysMCre-*Zfp36*$^{fl/fl}$; *Zfp36*$^{\Delta M}$ mice, targeting macrophages, neutrophils and monocytes), dendritic cells (CD11cCre-*Zfp36*$^{fl/fl}$;

Zfp36$^{\Delta DC}$) or epidermal cells (K14Cre-*Zfp36*$^{fl/fl}$; *Zfp36*$^{\Delta EP}$ mice) and subjected these mice to DMBA/TPA treatment. We observed a modest increase in tumor burden and size in *Zfp36*$^{\Delta DC}$ and *Zfp36*$^{\Delta M}$ mice as compared to control *Zfp36*$^{fl/fl}$ mice. In sharp contrast, we found that TTP deletion in epidermal cells (*Zfp36*$^{\Delta EP}$ mice) resulted in a dramatic increase in tumorigenesis. While control mice needed at least 8 weeks of TPA treatment for the development of the first papillomas, *Zfp36*$^{\Delta EP}$ mice displayed more rapid tumor formation (in less than 4 weeks), with major increases in tumor burden, size and progression to carcinoma (Figure 2B-C). In addition, the development of these tumors was accompanied by a gradual recruitment of neutrophils and, to a lesser extent, of IL17A-producing cells (mostly dermal γδ T cells) in the skin, indicating an essential role of TTP within keratinocytes in the control of inflammation-related carcinogenesis (Figure 2D). This was associated with upregulated expression of genes encoding cytokines (*Tnf* or *Il17f*), chemokines (*Cxcl1*, *Cxcl2*) and anti-microbial peptides (*Lcn2*, *S100a8*, *S100a9*) (Figure 2E). Taken together, these results highlight the key role of TTP within epidermal cells in the control of chronic inflammation and tumorigenesis.

Heightened tumor development upon epidermal-specific TTP ablation is not driven by dysregulated TNF production

TNF, whose mRNA is the best-characterized direct target of TTP (8), is involved in tumor promotion and progression in a wide range of genetic, chemically induced, and transplantable mouse models of cancer, including skin carcinogenesis (16). Since we observed dysregulated *Tnf* expression in the skin of DMBA/TPA-treated *Zfp36*$^{\Delta EP}$ mice, we generated mice with specific ablations of both TNF and TTP in keratinocytes (K14Cre*Tnf*$^{fl/fl}$*Zfp36*$^{fl/fl}$; *Zfp36*$^{\Delta EP}$*Tnf*$^{\Delta EP}$ mice). Using this approach, we previously demonstrated that the exacerbated imiquimod-induced skin inflammation seen in the *Zfp36*$^{\Delta EP}$ mice was strongly dependent on

the capacity of keratinocytes to produce TNF (11). In sharp contrast, these mice still displayed extreme sensitivity to DMBA/TPA-induced tumor formation, indicating that in this case, dysregulated production of TNF in the absence of TTP in epidermal cells is not the primary driver (Figure 3A). In addition, we performed similar experiments using neutralizing anti-TNF antibodies in *Zfp36*$^{\Delta EP}$ mice. Although we observed a decrease in tumor burden at early time-points, the numbers and sizes of the tumors were found to be comparable in isotype- and anti-TNF-treated *Zfp36*$^{\Delta EP}$ mice at later stages (Figure 3B). Nonetheless, we observed that accumulation of neutrophils and IL17A-producing γδ T cells was dependent on epidermal cell-derived TNF (Figure 3C). Furthermore, expression of inflammatory genes (*Tnf* but also *Cxcl2* or *Lcn2*) was also strongly reduced in these conditions as compared to *Zfp36*$^{\Delta EP}$ mice (Figure 3D). Taken together, these results suggest that a heightened inflammatory state is not central to increased tumorigenesis in these mice.

TTP regulates multiple key oncogenic pathways in neoplastic epidermal cells

While keratinocyte-derived TNF plays a dominant role in other disease settings, this does not seem to be the case in the current context of carcinogen-induced skin tumor formation. TTP can potentially control the mRNA stability of multiple inflammatory and oncogenic molecules. With the aim of defining the global impact of TTP in epidermal cells, we performed transcriptomic analysis. After induction of tumors in *Zfp36*$^{fl/fl}$ and *Zfp36*$^{\Delta EP}$ mice, we sorted EpCAM^{+}CD45^{-}CD140a^{-}CD31^{-} epidermal cells from papillomas at the same stage of development (as depicted in supplementary Figure S3). As comparators, we also sorted epidermal cells from adjacent DMBA/TPA-treated skin and from mock-treated animals. This allowed us to identify differentially expressed genes associated with chronic stimulation and/or specific to oncogenic transformation. Principal component analysis (PCA) showed a clear

segregation between neoplastic and adjacent/mock-treated samples (Figure 4A). Importantly, TTP-deficient and *Zfp36*$^{fl/fl}$ tumor cells tended to form separate clusters. Next, we performed pairwise comparisons. When comparing mock-treated *vs* tumor conditions, we identified 1100 and 1642 significantly upregulated genes in *Zfp36*$^{fl/fl}$ or *Zfp36*$^{\Delta EP}$ groups, respectively. We used the ARE-score algorithm to identify potential direct targets of TTP among dysregulated genes (Figure 4B) (17). When considering the genes that were upregulated in the *Zfp36*$^{\Delta EP}$ group, we observed a higher frequency of transcripts with an ARE score >2, in comparison to genes that were specifically increased in *Zfp36*$^{fl/fl}$ cells only. In line with the PCA data, we identified very few differentially expressed genes (DEGs) between *Zfp36*$^{fl/fl}$ and *Zfp36*$^{\Delta EP}$ groups in mock-treated conditions (3 genes) and DMBA/TPA non-tumoral skin (12 genes). Nevertheless, in this latter condition, we identified important inflammatory genes such as *Chil1*, *S100a8* and *S100a9*. Of note, expression of *Klk6*, the gene encoding a pro-inflammatory peptidase that promotes skin tumor formation and progression (18), was increased in TTP-deficient cells (Figure 4C). This was also the case for *Serpinb3a*, the gene encoding one of the squamous cell carcinoma antigen (SCCA)1-related molecules, commonly used as prognostic biomarkers in cancer patients (19).

For epidermal cells isolated from papillomas, using the same criteria, we identified 569 DEGs between *Zfp36*$^{fl/fl}$ and *Zfp36*$^{\Delta EP}$ groups. Apart from lipid metabolism, gene set enrichment analysis (GSEA) revealed few relevant pathways associated with genes that were down-regulated in TTP-deficient cells. In contrast, important pathways were enriched for genes that were up-regulated upon TTP ablation. As expected, we observed increased expression of genes involved in cytokine expression and activity, such as *Tnf*, *Il1b* and *Cxcl1*. We also noted dysregulation of key oncogenic processes including cell death, migration, proliferation and angiogenesis (Figure 4D). Among angiogenesis-related genes that were significantly

upregulated in *Zfp36*$^{\Delta EP}$ tumor cells, we identified key soluble factors such as *Vegfa* but also multiple genes involved in interactions with stromal cells (Figure 5A). To evaluate angiogenesis and neo-vascularization of *Zfp36*$^{fl/fl}$ and *Zfp36*$^{\Delta EP}$ papillomas, we performed immunofluorescent staining for VE-Cadherin (an endothelial marker) and endoglin, a transmembrane glycoprotein expressed on activated vascular endothelial cells (20). We observed increased density of endoglin^{+} cells in *Zfp36*$^{\Delta EP}$ papillomas as compared to *Zfp36*$^{fl/fl}$ samples, indicating that the absence of TTP in tumor cells promotes angiogenesis (Figure 5B). We conclude that TTP shapes the transcriptome of epidermal cells upon neoplastic transformation by controlling the expression of mRNAs associated with key oncogenic pathways such as neo-vascularization.

TTP destabilizes *Areg* mRNA in neoplastic epidermal cells

In order to identify direct potential targets of TTP in tumor cells, we looked at tumor-specific transcripts with an AREScore >2 that were significantly upregulated (FC>2) in the *Zfp36*$^{\Delta EP}$ group as compared to their control counterparts (Figure 6A). For selected genes, we validated our results by RT-qPCR on sorted epidermal cells from independent papilloma samples (Figure 6B). Several of these 60 genes were previously shown to be directly regulated by TTP in other cell types. These include genes encoding important cytokines, growth factors, chemokines or enzymes such as *Tnf* (21), *Csf2* (22), *Il1a* (10), *Lif* (23), *Vegfa* (4), *Cxcl1* (24) or *Mmp9* (25). We also identified several relevant mediators that, to the best of our knowledge, have not been reported as TTP targets. For example, we observed increased expression of *Pgf*, encoding placental growth factor, a VEGF homolog that plays an important role in ischemic, inflammatory, and malignant diseases (26). Along the same lines, we also highlight activinβA (*Inhba*), since this member of the TGFβ superfamily was shown to increase malignancy and metastatic spread of skin tumors (27); semaphorins (*Sema6d*, *Sema4d*), which can shape the tumor microenvironment (28); and ligands of the EGF receptor (*Areg*, *Ereg*). EGFR signalling

in epidermal cells plays an essential role downstream of the oncogenic RAS pathway (29). We therefore assessed whether *Areg* represents a *bona fide* TTP target.

We first performed in vitro experiments with primary *Zfp36*$^{fl/fl}$ and *Zfp36*$^{\Delta EP}$ keratinocytes. After a short incubation with TPA to induce TTP expression, we evaluated *Areg* mRNA half-life by treating the cells with actinomycin D and SB203580, the latter used to abrogate the inhibitory action of p38 MAPK on TTP activation (10). As shown in Figure 7A, *Areg* mRNA stability was strongly increased in *Zfp36*-deficient keratinocytes. Next, to assess if the putative ARE sequences found in the 3'UTR of the mRNA coding for AREG were sufficient to promote mRNA destabilization by TTP, we used a bidirectional reporter system (30) in which we inserted either the full-length 3'UTR sequence of *Areg*, or a truncated version lacking ARE motifs (Figure 7B). Plasmids containing a synthetic (AUUU)8 ARE motif (AU8) or no ARE (AU0) were used as controls. We evaluated the effect of TTP in co-transfection experiments in HEK293T cells. As expected, we observed a clear effect of TTP on the ratio between AU8 and AU0 reporter activities as compared with a control plasmid (expressing BOIP, encoded by *Ccdc89*) (Figure 7B). Similar conclusions were reached for the construct containing *Areg* 3'UTR, with and without ARE motifs.

To test the capacity of TTP to directly bind *Areg* ARE, we performed an electrophoretic mobility supershift assay. We incubated the *Areg* ARE probe with extracts from TTP-Flag expressing-HEK293T cells. Addition of α-Flag antibody resulted in a supershift that was not observed with BOIP-Flag or with an anti-V5 antibody, demonstrating that TTP physically interacts with the *Areg* mRNA ARE in this in vitro setting (Figure 7C). We confirmed the specificity of this binding by showing competition with increasing concentrations of cold *Areg* ARE but not with a control probe (Figure 7D). Finally, in order to define whether EGFR signalling plays a dominant role in the exacerbated tumorigenesis displayed by *Zfp36*$^{\Delta EP}$ mice, we treated them before each TPA application with the EGFR inhibitor AG1478. As shown in

Figure 7E, the number and size of the papillomas was greatly reduced upon treatment with this tyrosine kinase inhibitor. Taken together, these results indicate that TTP directly controls *Areg* mRNA stability in keratinocytes, and that dysregulated EGFR signaling may contribute to exacerbated tumor formation in *Zfp36*$^{\Delta EP}$ mice.

ZFP36 is downregulated in human squamous cell carcinoma

As our mouse models revealed a clear role of TTP in skin carcinogenesis, we investigated whether our observations might translate to the clinic. TTP is expressed in multiple cell types in the tumor microenvironment. To specifically look at the role of TTP in epidermal cells, we analyzed a recently published single-cell RNA-seq dataset of 18,359 keratinocytes taken from the skin of 7 control individuals and from 7 patients with cutaneous squamous cell carcinoma (cSCC) (31). As shown in Figure 8A, three major subpopulations were defined in normal skin. Based on the expression of representative genes, these were defined as basal (*COL17A1*), cycling (*MKI67*), and differentiating (*KRT1*) keratinocytes. cSCC exhibited four subpopulations, three recapitulating these normal epidermal states, and a tumor-specific keratinocyte (TSK) population with no counterpart in normal skin. These TSKs were shown to express epithelial-mesenchymal transition markers and to reside within a fibrovascular niche at leading edges of the tumor (31). We evaluated expression of *ZFP36* in these 7 cell clusters (Figure 8B). We observed lower expression in each of the three tumor subpopulations in comparison to their normal counterparts. In addition, its expression was further reduced in TSK cells. We observed very similar patterns for its 2 paralogs, *ZFP36L1* and *ZFP36L2*. In sharp contrast, expression of *ELAVL1*, that codes for another ARE-binding protein with opposite functions, was higher in tumor cells, and in particular in TSKs. We evaluated the signature scores for the 386 and 183 genes that were down- or up-regulated in TTP-deficient neoplastic

epidermal cells (as defined in Figure 4C). Consistent with their lower expression of *ZFP36*, TSKs exhibited the lowest and highest expression of these hallmark gene signatures, respectively (Figure 8C). Globally, these results suggest that ARE-mediated mRNA decay is dysregulated in human cSCC.

Discussion

We show here that TTP plays a major role in the pathogenesis of skin carcinogenesis. When its regulated expression was increased throughout the body by genetically removing the ARE instability elements that are located in its own mRNA 3'UTR (*Zfp36*$^{\Delta ARE}$ knock-in mice), DMBA/TPA-induced tumor burden was greatly reduced. Conversely, TTP ablation specifically in epidermal cells led to extreme sensitivity to DMBA/TPA-induced tumor formation. As TTP plays a major role in the control of inflammatory cytokine and chemokine expression, it was not surprising that both experimental situations were associated with important effects on tumor-associated inflammation. As previously demonstrated in the context of imiquimod-induced dermatitis (11), dysregulated production of TNF in the absence of TTP in epidermal cells was responsible for increased expression of inflammatory mediators and recruitment of innate immune cells during carcinogenesis; conversely, regulated TTP overexpression resulted in decreased skin infiltration of immune cells in this model (13). Wu *et al* (32) reported that calnineurin inhibitors downregulate TTP expression in keratinocytes. In line with our data, this led to increased expression of inflammatory mediators in HRas^{V12} transformed-keratinocytes. Malignant cell-derived TNF enhances the growth and spread of tumors in many different experimental models (33). However, the increased tumor development seen in *Zfp36*$^{\Delta EP}$ mice did not require keratinocyte-derived TNF production, indicating that TTP controls other pathways that play dominant roles in this model of tumorigenesis. As previously demonstrated in glioma cell lines (4), we could observe that neoplastic transformation of epidermal cells is accompanied by dysregulation of *Vegfa* expression, as well as that of *Pgf*, in the absence of TTP. This was associated with increased intratumoral angiogenesis. We also identified *Areg* mRNA as a direct target of TTP, and showed that inhibition of the EGFR pathway strongly decreased tumor burden in *Zfp36*$^{\Delta EP}$ mice. Of note, we also observed increased expression of *Ereg* (another EGFR ligand) and of *Adam12*, which acts as a "sheddase" for proHB-EGF (34).

The role of the EGFR pathway in skin tumorigenesis is complex. Transgenic AREG overexpression in keratinocytes leads to inflammatory epidermal hyperplasia without spontaneous development of skin tumors, suggesting that aberrant EGFR signalling is not sufficient to drive tumorigenesis (35). Rather, EGFR signalling functions as a survival factor during oncogenic transformation (36). It is also critical for Ras-dependent VEGF induction and angiogenesis (37) and contributes to the release of IL-1α, leading to the activation of NF-κB, the production of CXCR2 ligands and the suppression of keratinocyte differentiation (38). These results suggest that TTP activity in transformed cells could play a central role in reducing the oncogenic Ras/EGFR feed-forward loop that drives multiple aspects of tumor progression.

Ablation of TTP in hepatocytes was recently shown to decrease tumorigenesis upon diethylnitrosamine treatment, indicating that the effect of TTP on tumor initiation is context-dependent (39). It is possible that TTP plays a more important role in controlling tumor development at epithelial surfaces, as it is highly induced by inflammatory cues. We observed that expression of TTP was strongly heterogeneous in human malignant epidermal cells. Importantly, it was largely downregulated in a subset of tumor-specific keratinocytes that resides at the leading edges of the tumor in a fibrovascular niche (31). We can speculate that loss of TTP could contribute to the remodelling of the surrounding stroma through the regulation of key mediators known to promote angiogenesis (such as VEGF, PGF or MMPs) or activate cancer-associated fibroblasts (such as activinβA (40)). It would therefore be important to define the mechanisms leading to decreased *ZFP36*, *ZFP36L1* and *ZFP36L2* expression during skin tumor progression.

In conclusion, we have demonstrated that ARE-mediated mRNA decay, specifically that aspect regulated by TTP, controls key early steps of skin tumorigenesis in vivo. This pathway could therefore represent a valuable therapeutic target. More research is needed to understand the effects of TTP in the various aspects of tumor development identified in this study, as well

as others still to be discovered.

Methods

Mice. LoxP-flanked *Zfp36* mice (*Zfp36* $^{flox/flox}$) mice on C57BL/6 background were previously described (41). LysM-Cre (B6.129P2-*Lyz2*$^{tm1(cre)Ifo}$), CD11c-Cre (B6.Cg-Tg(Itgax-Cre)1-1Reiz) and K14-Cre (Tg(KRT14-cre)1Amc) mice on C57BL/6 backgrounds were purchased from The Jackson Laboratory. Cell-specific *Zfp36*-deficient mice were generated by crossing the *Zfp36* $^{flox/flox}$ mice with mice expressing Cre recombinase under the control of the murine M lysozyme promoter (*Zfp36*$^{\Delta M}$), the murine integrin alpha X promoter (*Zfp36*$^{\Delta DC}$) or the human keratin 14 promoter (*Zfp36*$^{\Delta EP}$). The double conditional *Zfp36*$^{\Delta EP}$*Tnf*$^{\Delta EP}$mice were obtained by mating *Zfp36*$^{\Delta EP}$mice with *Tnf* $^{flox/flox}$ mice, as previously described (11). *Zfp36*$^{\Delta ARE}$ and *Zfp36-V5* knock-in mice were previously described (13,15). All experiments were performed using littermates as controls. All mice were bred and maintained in a specific pathogen-free animal facility. All animal studies were approved by the local committees for animal welfare.

DMBA/TPA two-stage carcinogenesis.

For the experiments conducted with the *Zfp36*$^{\Delta ARE}$ mice and corresponding controls, seven week-old animals were anesthetized by inhalation of isoflurane, and the dorsal skin was shaved with surgical clippers and subsequently checked for the lack of hair growth. Initiation was accomplished by a single topical application of 400 nmol of 7,12-dimethylbenz[a]anthracene (DMBA) in 200 µl acetone. Promoter treatments with 10 nmol of 12-0 tetradecanoylphorbol-13-acetate (TPA) in 200 µl acetone, twice a week, were begun 1 week after initiation and continued for 20 weeks. Skin tumors induced by the initiation-promotion protocol were counted.

For all the other experiments conducted, eight week-old mice were anesthetized by i.p. injection of ketamine and xylazine and shaved on the back with an electrical shaver two days before

DMBA treatment. Mice were treated at days 0 and 3 or 7 with 80 or 200 nmol of DMBA in 200 µl acetone. *Zfp36*$^{\Delta EP}$, *Zfp36*$^{\Delta M}$ and *Zfp36*$^{\Delta DC}$ mice were treated at days 0 and 3 with 200 nmol of DMBA in 200 µl acetone, and *Zfp36*$^{\Delta EP}$*Tnf*$^{\Delta EP}$ mice were treated at days 0 and 7 with 80 nmol of DMBA in 200 µl acetone. At day 14, mice were treated twice per week with 6.5 nmol of TPA in 200 µl acetone for 12 to 40 weeks. Tumor incidence and burden were assessed once per week. The experiment was stopped when the tumors reached >10mm. Mice were euthanized when indicated, and skin samples were prepared for immunofluorescence, gene expression and flow cytometry analysis. When indicated, 500 µg/ml of AG1478 inhibitor in 200 µl acetone was applied 45 min before the TPA in 200 µl acetone, and 10 mg/kg of anti-TNF blocking antibodies (XT3.11 clone, BioXcell) in PBS was injected i.p. 3 times a week from week 1 to 10.

TPA treatment. The back skin of *Zfp36-V5* knock-in mice and *Zfp36* $^{flox/flox}$ was shaved 2 days before the start of the experiment. Then, these mice were treated with 6.5 nmol of TPA in 200 µl acetone on the back skin once a day for 3 days. Skin biopsies were collected 24h later to perform flow cytometry analysis.

Flow cytometry analysis. Skin samples were incubated for 16 h with dispase II (1 mg/ml, Sigma) and then with collagenase IV (1 mg/ml, Thermofisher) and DNase I (100 µg/ml, Sigma) for 45 min at 37°C. Cells were stained for CD45-FITC (clone 30-F11) and gamma delta TCR-PerCP-eFluor710 (clone eBio-GL3) from eBioscience; Ly6G- PerCP-Cy5.5 (clone 1A8), IL-17A-APC (clone TC11-18H10), CD3- (clone 17A2), CD19- (clone 1D3), Gr1-APC-Cy7 (clone RB6-8C5); CD11b- (clone M1/70), Ly6C- (clone AL-21), CD3-BV421 (clone 17A2) from BD Biosciences and V5 Tag-AF647 (Clone N/A, Catalog No: 46-1260) from Invitrogen.. Cells were incubated for 2h with PMA (25 ng/ml), ionomycin (500 ng/ml) and Brefeldin A (10 µg/ml)

and processed for intracellular staining using the Intracellular Fixation & Permeabilization kit (eBiosciences). Data were collected on a BD LSRII Fortessa and analyzed with FlowJoX software.

FACS isolation of cells. Tumors from mouse back skin were incubated for 2 h with collagenase I (Roche, 3.5 mg/ml) on a rocking plate at 37°C. Enzyme activity was blocked by adding EDTA (5 mM). Cells were stained for CD45-PE (clone 30-F11) from eBioscience, CD140a-APC (clone APA5) and CD31-APC (clone MEC13.1) from BD Biosciences and CD326-APC-Cy7 (clone G8.8) from Imtec. Living cells from tumors, DMBA/TPA-treated and mock-treated skin samples were selected by Live/dead aqua dye exclusion (Invitrogen). Then, EpCAM (CD326)-positive cells were selected after CD140a, CD31 and CD45 exclusion. Sorting was performed on BD FACSAria II and analyzed with FACSDiva software.

Cell culture. Mouse primary keratinocytes were isolated from newborn mice (24-72 h post-birth) as described by Li *et al* (42). Cells were maintained in complete Keratinocyte Growth Medium II (Promocell GmbH, Germany) at 36°C and 7% CO_2. HEK293T cells (ATCC) were maintained in DMEM medium containing 10% FBS, 50 U/ml Penicillin, 50µg/ml Streptamycin and 1mM sodium pyruvate (Gibco). Transfections were performed using the calcium phosphate method of transfection. Plasmid DNA was added to a $CaCl_2$ solution, then added dropwise into a Hepes-buffered phosphate solution. This DNA solution is then incubated at room temperature for 30 min before being spotted on the cell culture. Cells' medium was changed prior to adding the DNA and after incubation of the cells overnight with the DNA mixture.

Dual reporter plasmids. Plasmids containing the WT Globin 3'UTR (AU0 = no ARE) or Globin

3'UTR with AU rich insertion $(AUUU)_8$ (AU8 = canonical ARE sequence) were used as controls. The plasmids also contain the sequence coding for the *Firefly* luciferase (F-Luc) as a transfection efficiency control. Both luciferases are under the control of a bidirectional CMV promoter.

The WT 3'UTR of *Areg* gene was amplified by RT-PCR using the primers 5'- agctagagcggccgcggatccCTGAGGACAATGCAGGGTAAA-3' and 5'gctcgaagcggccgcTGTTTAAAAAAAGTTTAATGAGCTATA-3', then cloned into the NotI site of the AU_0 plasmid from Barreau et al.(30), using a ligation independent cloning (LIC) method. For *Areg*ΔARE, a DNA fragment containing the 3'UTR of *Areg* without the putative ARE motifs was synthesized (Integrated DNA Technologies), then amplified by PCR before cloning in the AU_0 plasmid.

Electrophoretic mobility shift assay. Analysis of possible *Areg* mRNA-TTP interactions by supershift assay was performed as described in (43) with the following modifications. Cell extracts from HEK293T cells transfected with TTP-Flag of BOIP-Flag were incubated with ^{32}P-labelled RNA probe, followed by the addition of anti-V5 or anti-Flag antibody. Areg probe corresponding to *Areg* 3'UTR AU-rich region (Figure 7B, underlined sequence) and control probe corresponding to pBS polylinker region were produced by in vitro transcription using T7 RNA polymerase and ^{p32}UTP. Samples were loaded on 5% polyacrylamide non-denaturing gels containing 6% glycerol and 0.5X TBE at 7.5 mA for 16 hours at 4°C. Competition experiments were performed by adding 2, 4, 8, 16 or 32 fold molar excess of unlabeled Areg probe or control pBS probe.

Gene expression (2 step qPCR). Total RNA was extracted with the RNeasy Minikit (Qiagen) and reverse-transcribed with the High-Capacity cDNA Archive Kit (Applied Biosystems).

cDNA was amplified using SYBR green or TaqMan probes. Primer sequences are described in supplemental Table 1.

Immunofluorescence staining. Tumors from mouse tissues were embedded and frozen in OCT (Tissue-Tek). Sections (6 µm) were stained as explained in (44). Anti-Endoglin (CD105, polyclonal, R&D), anti-Keratin 14 (clone SIG-3476, Thermofisher) and anti-VE-Cadherin (CD144, clone 11D4.1, BD Bioscience) were used as primary antibodies.The following secondary antibodies were used: anti-goat, anti-rat, anti-rabbit conjugated to AlexaFluor488 (Molecular Probes), to rhodamine Red-X (JacksonImmunoResearch) or to Cy5 (Jackson ImmunoResearch) respectively. Nuclei were stained in Hoechst solution. Slides were observed at 200-fold magnification. Images were acquired using Zeiss AxioImager M1 and analyzed with Zen 2.3 lite Blue software.

RNA sequencing. For the RNA-Seq analysis of skin biopsies from the *Zfp36*$^{\Delta ARE}$ mice and their corresponding controls, full-thickness skin biopsies were taken at the end of the experiment. These were all from treated but non-tumoral skin. Total RNA was isolated by pestle homogenization using a TRIzol and chloroform method according to the manufacturer's instructions (Invitrogen). Raw pair-end fastq files were provided by the sequencing contractor, Q2Labsolutions.com. Low quality sequence reads with mean score <20 were removed using a custom perl script. The processed reads were mapped to the mm10 genome using the Spliced Transcripts Alignment to a Reference (STAR) software (v2.5.2b) (45). The number of fragments per gene were counted using the featureCounts command available from Subread (v1.5.0-p1) (46). Differential gene expression analysis was performed using the R package DESeq2 (version 1.12.4) (47).

Total RNA from sorted epidermal cells (isolated from mock-treated skin, DMBA/TPA-treated adjacent skin and papillomas) was extracted using an RNeasy Plus Micro Kit (Qiagen). Quality control, library preparation and RNA sequencing were performed by BRIGHTcore ULB-VUB, Belgium (http:\\www.brightcore.be). RNA sequencing was performed on triplicates of each group, using the standard Illumina HiSeq sequencing protocol ($20x10^6$ reads/sample). FastQC was used for read quality determination. Differential gene expression analysis was done using the EdgeR method, with FDR <0.05 and fold change as indicated.

ARE Score analysis was performed according to the scoring option (http://AREScore.dkfz.de/AREScore.pl) (17). We first defined a list of genes differentially expressed in tumors from *Zfp36*$^{\Delta EP}$ mice compared to tumors from *Zfp36*$^{fl/fl}$ mice (minimal read count of 10 in RNA-Seq). We extracted all isoforms of described transcripts from the RefSeq database.

scRNA-seq Analysis. We retrieved single cell transcriptomic profiles of 7 normal skin and 7 cutaneous squamous cell carcinoma from a recently published dataset (31) (accession number: GSE144236). We restricted our analysis to epithelial cells including the following subpopulations: normal keratinocytes (basal, cycling, and differentiating), tumor keratinocytes (basal, cycling, and differentiating and tumor-specific keratinocytes) to obtain a total of 18359 cells. A Seurat object was created using Seurat r package v3.2.2 and cells-metadata, established by the authors (31), was added by applying *AddMetaData* function. Counts were normalized with SCTransform method by which we regressed mitochondrial mapped genes and UMI counts. We ran the dimensionality reduction functions (*RunPCA* and *RunUMAP)* with the first 15 PCs as input. A Shared Nearest Neighbor (SNN) Graph and Seurat clusters were identified. Cluster annotation was done according to the added cells-metadata. To visualize the reduced dimension coordinates of the annotated cells we used the *DimPlot* function and gene expression was assessed using *FeaturePlot* and *VlnPlot* functions. To determine the enrichment of

differentially expressed genes in WT or *Zfp36*$^{\Delta EP}$ tumor cells obtained from our bulk RNA-seq data, two gene lists were created, and enrichment score was measured by applying the *AddModuleScore* Seurat-function.

Statistics. Results are expressed as means ± SEM. The statistical significance was assessed as indicated using GraphPad Prism 8.0. A P value less than 0.05 was considered significant.

Study approval

Animal studies performed in Belgium were approved by the institutional Animal Care and local committee for animal welfare of the BIOPOLE ULB CHARLEROI. Animal studies performed at the National Cancer Institute were approved by the Institutional Animal Care and Use Committee (IACUC) of National Cancer Institute (Frederick, Maryland) and were conducted in accordance with the IACUC guidelines and the National Institutes of Health Guide for the Care and Use of Laboratory Animals (National Institutes of Health Publication No. 86–23, 1985). Animals were maintained in a specific pathogen-free facility with *ad libitum* access to water and feed. All animals were used in scientific experiments for the first time.

Data Availability

Raw RNA-Seq data can be accessed on GEO (accession numbers : GSE148199 and GSE151587).

Acknowledgments

This study was supported by the Fonds National de la Recherche Scientifique (FRS-FNRS, Belgium), the Fondation Contre le Cancer, by the European Regional Development Fund (ERDF) of the Walloon Region (Wallonia-Biomed portfolio, 411132-957270), the "Actions de Recherches Concertées" (AV.12/17), the Intramural Research Program of the NIH, NIEHS and NCI, and the Télévie. SG is a senior research associate of the FRS-FNRS. CL and AA were supported by PhD fellowship from the FRS-FNRS and the Télévie, respectively. BdT was supported by a PhD fellowship of the Belgian Fonds pour la Recherche en Industrie et Agriculture (FRIA). We thank Marion Splittgerber and Frédérick Libert (IRIBHM and Bright

Core NGS platform) for preliminary RNA-Seq analysis. The graphical abstract was created with BioRender.com.

Author Contributions

AA, IDV and LVM conducted most of the experiments. RS, BS, LZ, AAz, CL, MM, CG and WSF contributed to some experiments; MN and ST provided technical help for the experiments. AAz, BdT and LZ performed transcriptomic analysis. AA analysed the data and prepared the figures. CB, CG, VK and GT provided input for research design and interpretation. WH provided critical reagents. SG and PJB supervised the work and wrote the manuscript. All authors were involved in critically revising the manuscript for important intellectual content. All authors had full access to the data and approved the manuscript before it was submitted by the corresponding author.

Competing Interests

The authors declare no competing interests.

1. Hitti E, Bakheet T, Al-Souhibani N, Moghrabi W, Al-Yahya S, Al-Ghamdi M, et al. Systematic analysis of AU-rich element expression in cancer reveals common functional clusters regulated by key RNA-binding proteins. Cancer Res. 2016;

2. Gebeshuber CA, Zatloukal K, Martinez J. miR-29a suppresses tristetraprolin, which is a regulator of epithelial polarity and metastasis. EMBO Rep. 2009;10:400–5.

3. Sohn BH, Park IY, Lee JJ, Yang S-J, Jang YJ, Park KC, et al. Functional switching of TGF-beta1 signaling in liver cancer via epigenetic modulation of a single CpG site in TTP promoter. Gastroenterology. 2010;138:1898–908.

4. Suswam E, Li Y, Zhang X, Gillespie GY, Li X, Shacka JJ, et al. Tristetraprolin down-regulates interleukin-8 and vascular endothelial growth factor in malignant glioma cells. Cancer Res. 2008;68:674–82.

5. Upadhyay R, Sanduja S, Kaza V, Dixon DA. Genetic polymorphisms in RNA binding proteins contribute to breast cancer survival. Int J Cancer. 2013;132:E128–38.

6. Rounbehler RJ, Fallahi M, Yang C, Steeves M a., Li W, Doherty JR, et al. Tristetraprolin impairs Myc-induced lymphoma and abolishes the malignant state. Cell. 2012;150:563–74.

7. Coelho MA, de Carné Trécesson S, Rana S, Zecchin D, Moore C, Molina-Arcas M, et al. Oncogenic RAS Signaling Promotes Tumor Immunoresistance by Stabilizing PD-L1 mRNA. Immunity. 2017;47:1083-1099.e6.

8. Carballo E, Lai WS, Blackshear PJ. Feedback inhibition of macrophage tumor necrosis factor-alpha production by tristetraprolin. Science. 1998;281:1001–5.

9. Taylor G a, Carballo E, Lee DM, Lai WS, Thompson MJ, Patel DD, et al. A pathogenetic role for TNF alpha in the syndrome of cachexia, arthritis, and autoimmunity resulting from tristetraprolin (TTP) deficiency. Immunity. 1996;4:445–54.

10. Kratochvill F, Machacek C, Vogl C, Ebner F, Sedlyarov V, Gruber AR, et al. Tristetraprolin-driven regulatory circuit controls quality and timing of mRNA decay in inflammation. Mol Syst Biol. 2011;7:560.

11. Andrianne M, Assabban A, La C, Mogilenko D, Salle DS, Fleury S, et al. Tristetraprolin expression by keratinocytes controls local and systemic inflammation. JCI Insight. 2017;2:1–16.

12. Molle C, Zhang T, Ysebrant de Lendonck L, Gueydan C, Andrianne M, Sherer F, et al. Tristetraprolin regulation of interleukin 23 mRNA stability prevents a spontaneous inflammatory disease. J Exp Med. 2013;210:1675–84.

13. Patial S, Curtis AD, Lai WS, Stumpo DJ, Hill GD, Flake GP, et al. Enhanced stability of tristetraprolin mRNA protects mice against immune-mediated inflammatory pathologies. Proc Natl Acad Sci U S A. 2016;113:1865–70.

14. Abel EL, Angel JM, Kiguchi K, DiGiovanni J. Multi-stage chemical carcinogenesis in mouse skin: Fundamentals and applications. Nat Protoc. 2009;4:1350–62.

15. Zhang X, Chen X, Liu Q, Zhang S, Hu W. Translation repression via modulation of the cytoplasmic poly(A)-binding protein in the inflammatory response. Elife. 2017;6.

16. Balkwill F. Tumour necrosis factor and cancer. Nat Rev Cancer. 2009;9:361–71.

17. Spasic M, Friedel CC, Schott J, Kreth J, Leppek K, Hofmann S, et al. Genome-wide assessment of AU-rich elements by the AREScore algorithm. PLoS Genet. 2012;8:e1002433.

18. Khoury N, Zingkou E, Pampalakis G, Sofopoulos M, Zoumpourlis V, Sotiropoulou G. KLK6 protease accelerates skin tumor formation and progression. Carcinogenesis. 2018;39:1529–36.

19. Turato C, Scarpa M, Kotsafti A, Cappon A, Quarta S, Biasiolo A, et al. <scp>S</scp> quamous cell carcinoma antigen 1 is associated to poor prognosis in esophageal cancer through immune surveillance impairment and reduced chemosensitivity. Cancer Sci. 2019;110:1552–63.

20. Dallas NA, Samuel S, Xia L, Fan F, Gray MJ, Lim SJ, et al. Endoglin (CD105): a marker of tumor vasculature and potential target for therapy. Clin Cancer Res. 2008;14:1931–7.

21. Lai WS, Carballo E, Strum JR, Kennington E a, Phillips RS, Blackshear PJ. Evidence that tristetraprolin binds to AU-rich elements and promotes the deadenylation and destabilization of tumor necrosis factor alpha mRNA. Mol Cell Biol. 1999;19:4311–23.

22. Carballo E, Lai WS, Blackshear PJ. Evidence that tristetraprolin is a physiological regulator of granulocyte-macrophage colony-stimulating factor messenger RNA deadenylation and stability. Blood. 2000;95:1891–9.

23. Qiu L-Q, Lai WS, Bradbury A, Zeldin DC, Blackshear PJ. Tristetraprolin (TTP) coordinately regulates primary and secondary cellular responses to proinflammatory stimuli. J Leukoc Biol. 2015;97:723–36.

24. Datta S, Biswas R, Novotny M, Pavicic PG, Herjan T, Mandal P, et al. Tristetraprolin regulates CXCL1 (KC) mRNA stability. J Immunol. 2008;180:2545–52.

25. Van Tubergen EA, Banerjee R, Liu M, Broek R V., Light E, Kuo S, et al. Inactivation or Loss of TTP Promotes Invasion in Head and Neck Cancer via Transcript Stabilization and Secretion of MMP9, MMP2, and IL-6. Clin Cancer Res. 2013;19:1169–79.

26. Van de Veire S, Stalmans I, Heindryckx F, Oura H, Tijeras-Raballand A, Schmidt T, et al. Further Pharmacological and Genetic Evidence for the Efficacy of PlGF Inhibition in Cancer and Eye Disease. Cell. 2010;141:178–90.

27. Antsiferova M, Huber M, Meyer M, Piwko-czuchra A, Ramadan T, Macleod AS, et al. Activin enhances skin tumourigenesis and malignant progression by inducing a pro-tumourigenic immune cell response. Nat Commun. Nature Publishing Group; 2011;2:510–76.

28. Franzolin G, Tamagnone L. Semaphorin Signaling in Cancer-Associated Inflammation. Int J Mol Sci. 2019;20.

29. Dlugosz AA, Hansen L, Cheng C, Alexander N, Denning MF, Threadgill DW, et al. Targeted disruption of the epidermal growth factor receptor impairs growth of squamous papillomas expressing the v-ras(Ha) oncogene but does not block in vitro keratinocyte responses to oncogenic ras. Cancer Res. 1997;57:3180–8.

30. Barreau C, Watrin T, Beverley Osborne H, Paillard L. Protein expression is increased by a class III AU-rich element and tethered CUG-BP1. Biochem Biophys Res

Commun. 2006;347:723–30.

31. Ji AL, Rubin AJ, Thrane K, Jiang S, Reynolds DL, Meyers RM, et al. Multimodal Analysis of Composition and Spatial Architecture in Human Squamous Cell Carcinoma. Cell. 2020;182:497-514.e22.

32. Wu X, Tommasi Di Vignano A, Zhou Q, Michel-Dziunycz PJ, Bai F, Mi J, et al. The ARE-binding protein Tristetraprolin (TTP) is a novel target and mediator of calcineurin tumor suppressing function in the skin. 2018;1–22.

33. Crusz SM, Balkwill FR. Inflammation and cancer: advances and new agents. Nat Rev Clin Oncol. 2015;12:1–13.

34. Wang J, Zhang Z, Li R, Mao F, Sun W, Chen J, et al. ADAM12 induces EMT and promotes cell migration, invasion and proliferation in pituitary adenomas via EGFR/ERK signaling pathway. Biomed Pharmacother. 2018;97:1066–77.

35. Dahlhoff M, Schneider MR. Transgenic mouse lines help decipher the roles of EGFR ligands in the skin. Exp Dermatol. 2016;25:185–6.

36. Sibilia M, Fleischmann A, Behrens A, Stingl L, Carroll J, Watt FM, et al. The EGF Receptor Provides an Essential Survival Signal for SOS-Dependent Skin Tumor Development. Cell. 2000;102:211–20.

37. Casanova ML, Larcher F, Casanova B, Murillas R, Fernández-Aceñero MJ, Villanueva C, et al. A critical role for ras-mediated, epidermal growth factor receptor-dependent angiogenesis in mouse skin carcinogenesis. Cancer Res. 2002;62:3402–7.

38. Cataisson C, Salcedo R, Hakim S, Moffitt BA, Wright L, Yi M, et al. IL-1R-MyD88 signaling in keratinocyte transformation and carcinogenesis. J Exp Med. 2012;209:1689–702.

39. Kröhler T, Kessler SM, Hosseini K, List M, Barghash A, Patial S, et al. The mRNA-binding Protein TTP/ZFP36 in Hepatocarcinogenesis and Hepatocellular Carcinoma. Cancers (Basel). 2019;11.

40. Nagaraja AS, Dood RL, Armaiz-Pena G, Kang Y, Wu SY, Allen JK, et al. Adrenergic-mediated increases in INHBA drive CAF phenotype and collagens. JCI Insight. 2017;2.

41. Qiu L-Q, Stumpo DJ, Blackshear PJ. Myeloid-specific tristetraprolin deficiency in mice results in extreme lipopolysaccharide sensitivity in an otherwise minimal phenotype. J Immunol. 2012;188:5150–9.

42. Li L. Mouse Epidermal Keratinocyte Culture. In: Randell SH, Fulcher ML, editors. Epithel Cell Cult Protoc Second Ed. Totowa, NJ: Humana Press; 2013. page 177–91.

43. Gueydan C, Houzet L, Marchant A, Sels A, Huez G, Kruys V. Engagement of tumor necrosis factor mRNA by an endotoxin-inducible cytoplasmic protein. Mol Med. 1996;2:479–88.

44. Lapouge G, Beck B, Nassar D, Dubois C, Dekoninck S, Blanpain C. Skin squamous cell carcinoma propagating cells increase with tumour progression and invasiveness. EMBO J. 2012;31:4563–75.

45. Dobin A, Davis CA, Schlesinger F, Drenkow J, Zaleski C, Jha S, et al. STAR: ultrafast universal RNA-seq aligner. Bioinformatics. 2013;29:15–21.

46. Liao Y, Smyth GK, Shi W. featureCounts: an efficient general purpose program for assigning sequence reads to genomic features. Bioinformatics. 2014;30:923–30.

47. Love MI, Huber W, Anders S. Moderated estimation of fold change and dispersion for RNA-seq data with DESeq2. Genome Biol. BioMed Central; 2014;15:550.

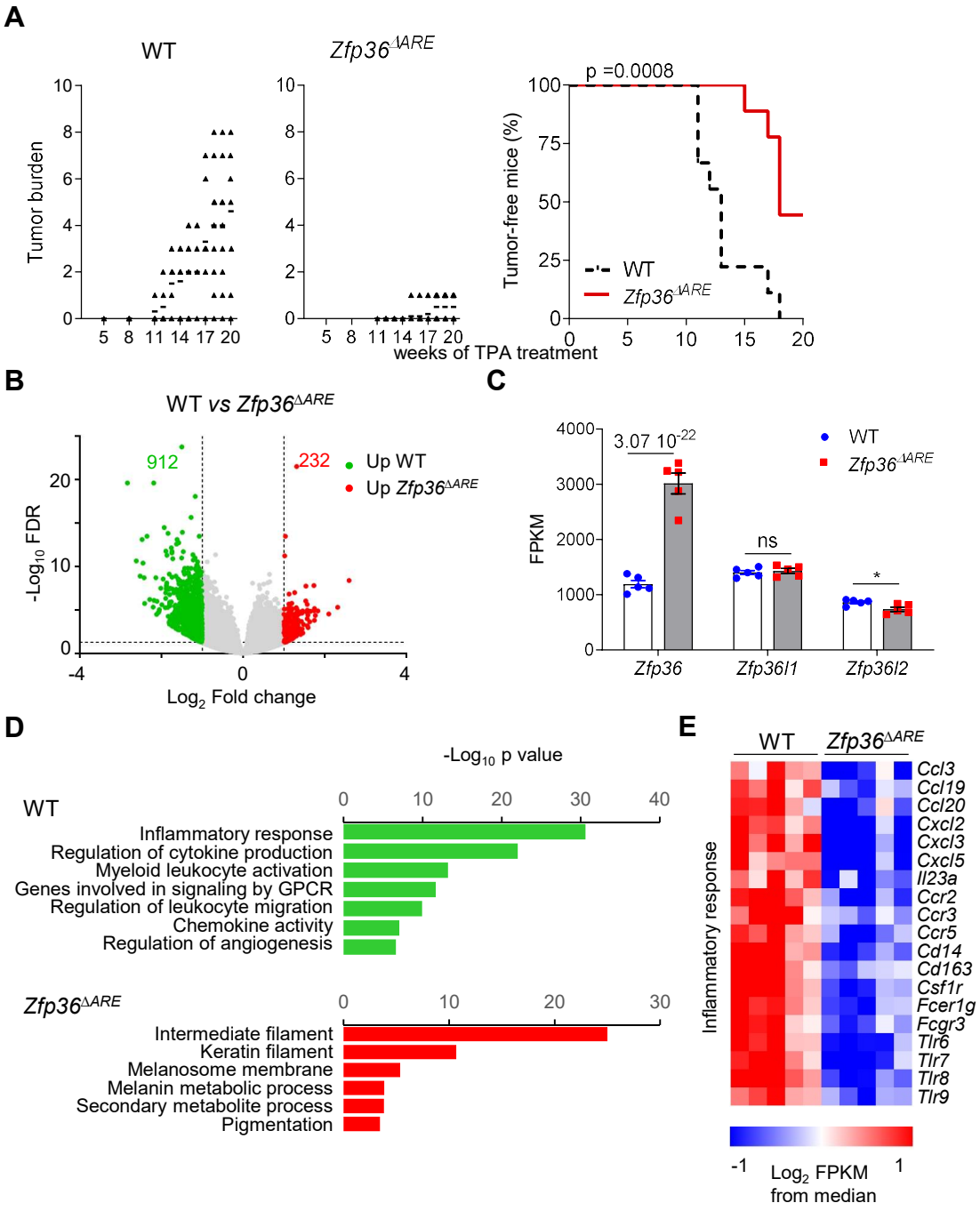

Figure 1: Regulated overexpression of endogenous TTP protects mice from cutaneous chemical carcinogenesis. *Zfp36*$^{\Delta ARE}$ mice and their controls (WT) were treated on shaved back skin with DMBA/TPA. They were monitored for 20 weeks at weekly intervals for tumor development. (A) Average tumor burdens and Kaplan-Meier curves describing tumor-free mice are shown for both groups (n = 9, representative of 2 experiments). (B) RNA-Seq analysis on adjacent, treated but non-tumoral whole-thickness skin samples from both groups (n = 5). Differentially expressed genes are shown in the volcano plot in red if upregulated in *Zfp36*$^{\Delta ARE}$ skin (232 genes) or in green in WT skin (912 genes) among all 1144 genes that met the fold change (Fold change > 2) and significance criteria (FdR < 0.05) (shown in grey). (C) *Zfp36* and other TTP family member mRNA expression in WT and *Zfp36*$^{\Delta ARE}$ mice, based on the RNA-Seq data from non-tumoral adjacent skin samples. (D) Gene set enrichment analysis of the most significantly enriched pathways in *Zfp36*$^{\Delta ARE}$ (red) or in WT (green) samples. (E) Heatmap of expression levels of inflammatory response genes significantly increased or decreased in treated *Zfp36*$^{\Delta ARE}$ or WT skin. Statistical analysis (*p < 0.05) was assessed by Mantel-Cox log-rank test indicating differences between all groups (p value = 0.0008) (A) and using DeSeq2 (FdR = 3.07 10^{-22}) (C). ns: not significant.

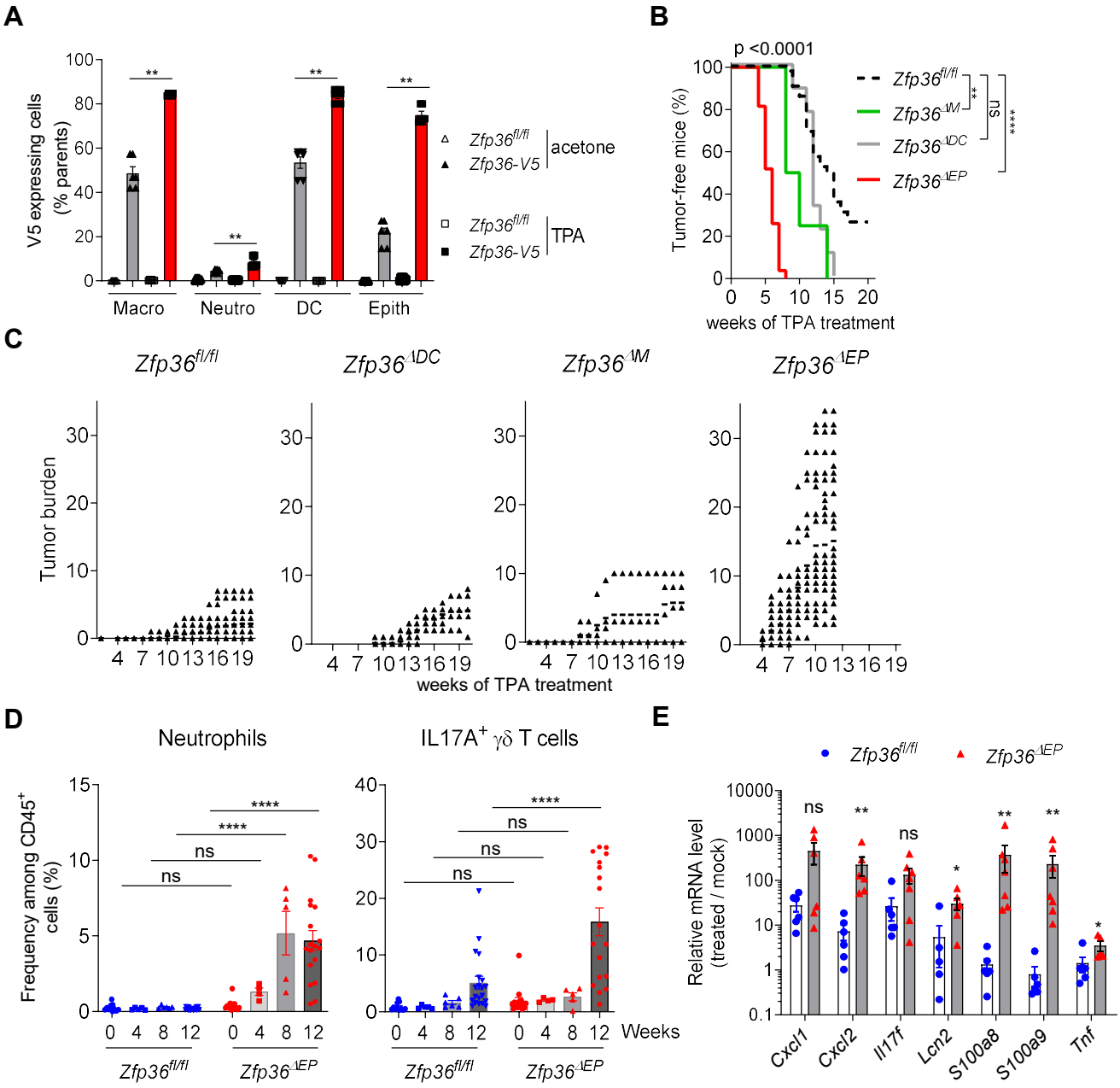

Figure 2: TTP expressed by keratinocytes controls skin tumorigenesis. *Zfp36-V5* and *Zfp36$^{fl/fl}$* mice were treated for 3 days with TPA or acetone on shaved back skin (A). *Zfp36$^{\Delta DC}$*, *Zfp36$^{\Delta M}$*, *Zfp36$^{\Delta EP}$* mice and their littermate controls (*Zfp36$^{fl/fl}$*) were topically treated on back skin with DMBA/TPA for 12 to 20 weeks, and monitored every week for tumor formation. The experiment was stopped when the tumors reached >10mm (B-E). (A) Ratio of V5-expressing skin cells in each condition analyzed by flow cytometry: macrophages, neutrophils, DCs and epithelial cells (keratinocytes). Data are shown as percentage of the initial population (mean ± SEM, n = 6, representative of 2 experiments). (B) Kaplan-Meier plot of DMBA/TPA-treated mice depicting papilloma-free state post-TPA promotion (n = 4-42, pool of 6 experiments). (C) Tumor burdens of *Zfp36$^{fl/fl}$*, *Zfp36$^{\Delta EP}$*, *Zfp36$^{\Delta M}$ and Zfp36$^{\Delta DC}$* back skins. (D) Kinetics of cell infiltration in total back skin from *Zfp36$^{\Delta EP}$* mice: neutrophils and IL-17A-producing γδT cells among CD45$^+$ cells are shown by intracellular protein staining. Results are given as mean ± SEM (n= 4-27, pool of 4 experiments). Gating strategy for flow cytometry is presented in supplemental Figures S1 and S2. (E) Skin samples, including tumors, from *Zfp36$^{\Delta EP}$* and their littermate mice were collected for analysis of transcript levels by qPCR at 12 weeks of DMBA/TPA treatment. Results are expressed as relative to the *Zfp36$^{fl/fl}$* mock group, which was arbitrarily set to 1 (mean ± SEM, n = 7). Statistical significance (*$p < 0.05$, **$p < 0.01$, ****$p < 0.0001$) was assessed by 2-tailed Mann-Whitney test (A, E), by Mantel-Cox log-rank test and pairwise comparisons indicating differences between deficient mice compared to their controls (B) or by the one-way ANOVA test with Bonferroni correction compared to the *Zfp36$^{fl/fl}$* group (D) . ns: not significant.

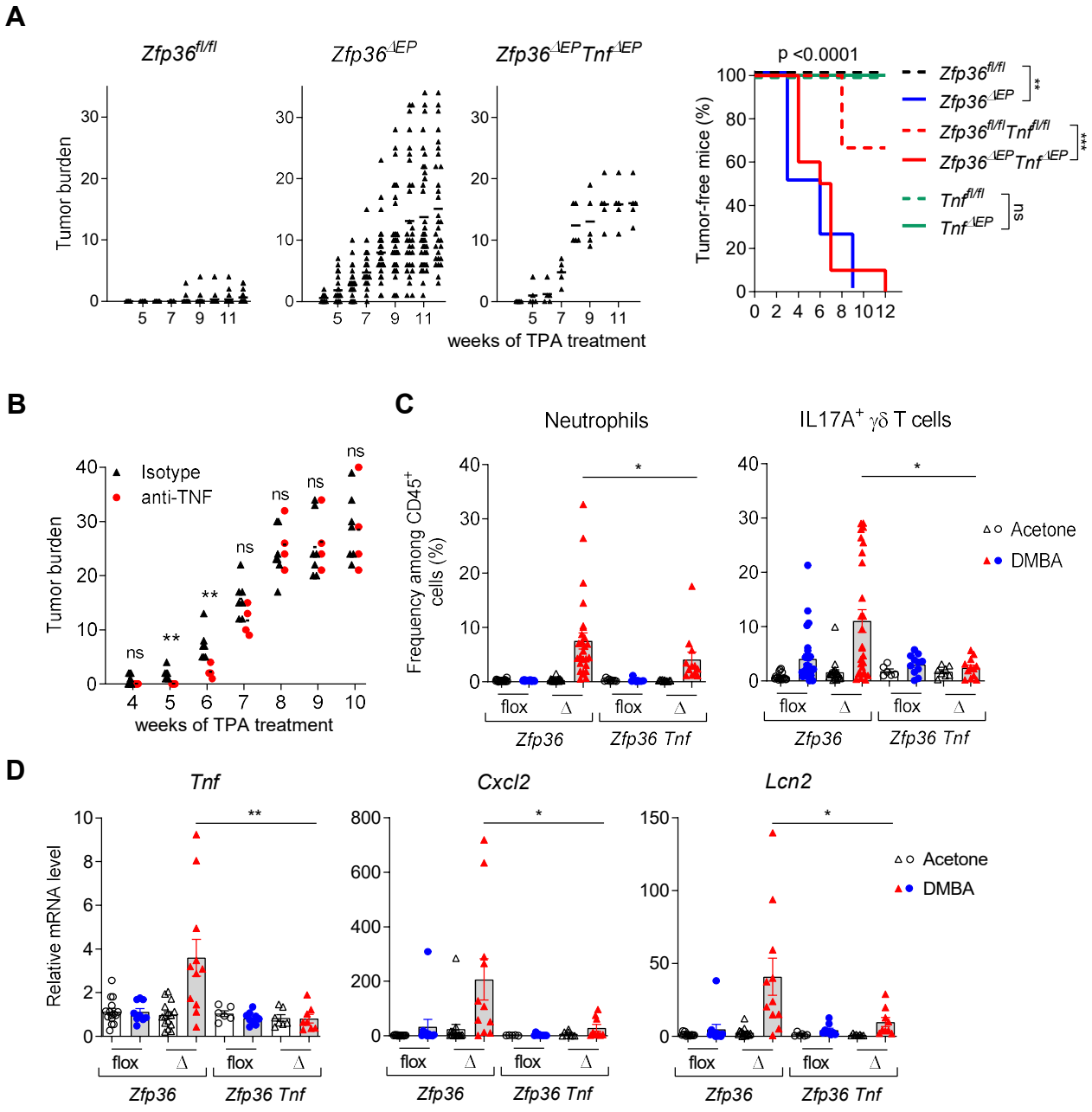

Figure 3: Dysregulated production of TNF in the absence of TTP in keratinocytes does not critically contribute to the sensitivity of *Zfp36*$^{\Delta EP}$ mice to tumor development. Tumors from *Zfp36*$^{\Delta EP}$*Tnf*$^{\Delta EP}$ (red), *Tnf*$^{\Delta EP}$ (green), *Zfp36*$^{\Delta EP}$ (blue) and littermates (dotted lines) mice were monitored during 12-20 weeks after DMBA/TPA treatment. (A) Incidence and size of tumors of all groups. Kaplan-Meier curves showing tumor-free mice during the experiment (n = 4-11, pool of 2 experiments). (B) DMBA/TPA-treated *Zfp36*$^{\Delta EP}$ mice received anti-TNFa or control isotype (n = 4-5, representative of one experiment). (C) Cell recruitment in total back skin was analyzed by flow cytometry (mean ± SEM, n = 4-11, pool of 2 experiments). Gating strategy for flow cytometry is presented in supplemental Figure S2. (D) Total back skin was collected for gene expression analysis by qPCR. Deficient mice (Δ) and their littermates (flox) are shown for both groups. Levels of *Tnf*, *Cxcl2* and *Lcn2* mRNAs were measured for each condition. Values from mock skin of corresponding controls were normalized against *Actb* and arbitrarily set at 1 (mean ± SEM, n = 6-11). Statistical significance (**p* < 0.05, ***p* < 0.01, ***p < 0.001) was assessed by Mantel-Cox log-rank and pairwise comparisons (A), by 2-tailed Mann-Whitney test (B, C, D). ns: not significant.

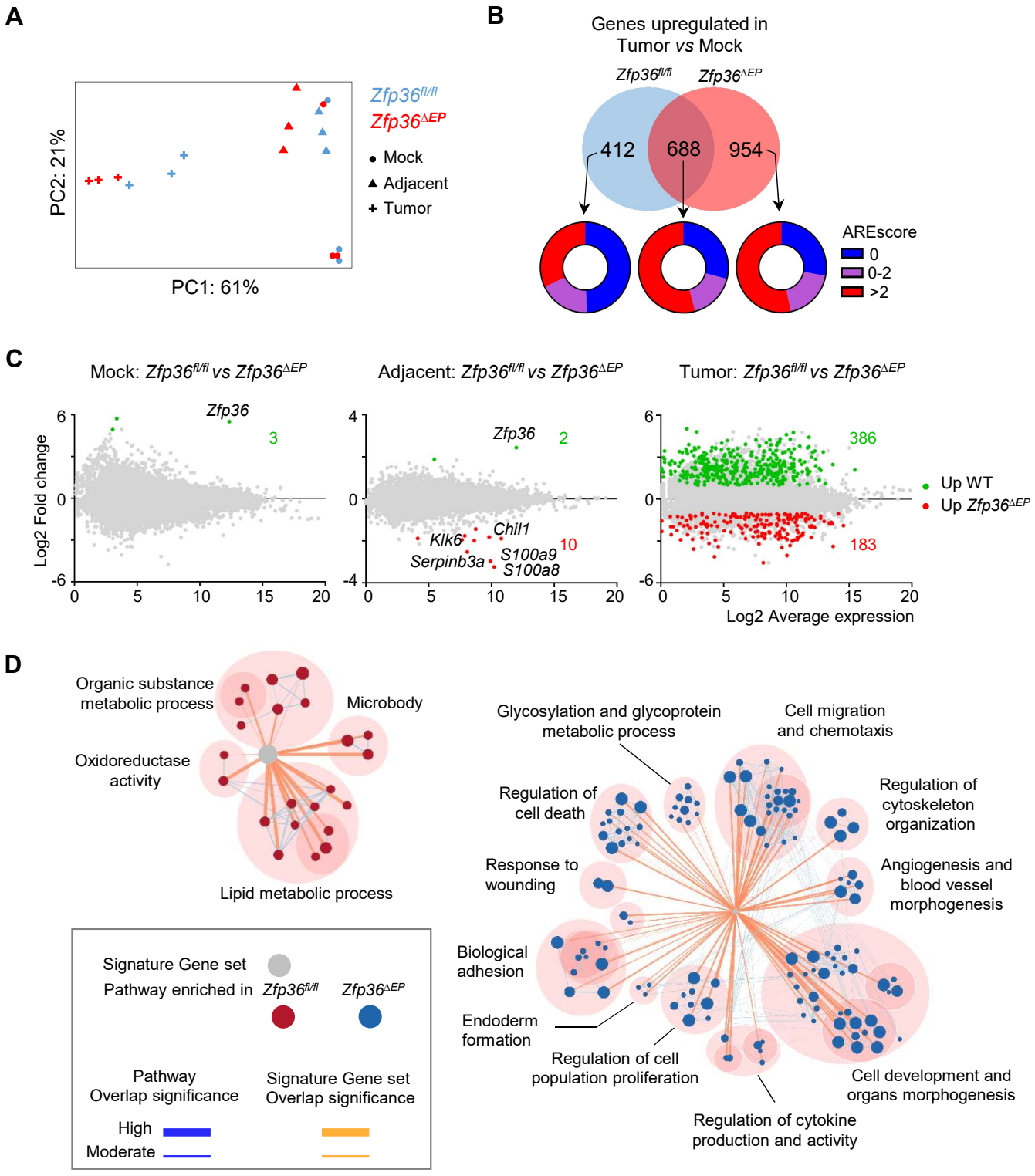

Figure 4: TTP shapes the transcriptome of epidermal cells upon neoplastic transformation. Epithelial cells from tumors, adjacent-treated and mock-treated skin of *Zfp36*$^{\Delta EP}$ (red) and littermates (blue) mice were isolated by flow cytometry after DMBA/TPA treatment for RNA-Seq analysis (n = 3). (A) PCA analysis showing segregation of samples. (B) Number of genes upregulated in tumors compared to mock skin samples. AREscore frequencies of dysregulated genes are shown for the indicated categories. (C) M-A plots indicating up- (red) and down- (green) regulated genes in *Zfp36*$^{\Delta EP}$ for cells isolated from mock-treated skin, adjacent-treated skin, and tumors. (D) Differentially Expressed Genes analysis of *Zfp36*$^{fl/fl}$ (WT, red) and *Zfp36*^{DEP} (blue) tumor cells. Signature Gene sets represent upregulated genes in WT tumors (386 genes, left part) and *Zfp36*^{DEP} (183 genes, right part). Overlaps between pathways are indicated in blue lines, and the overlaps between signature gene sets is indicated in orange. The thicker the line is, the more enriched genes are present between the two pathways.

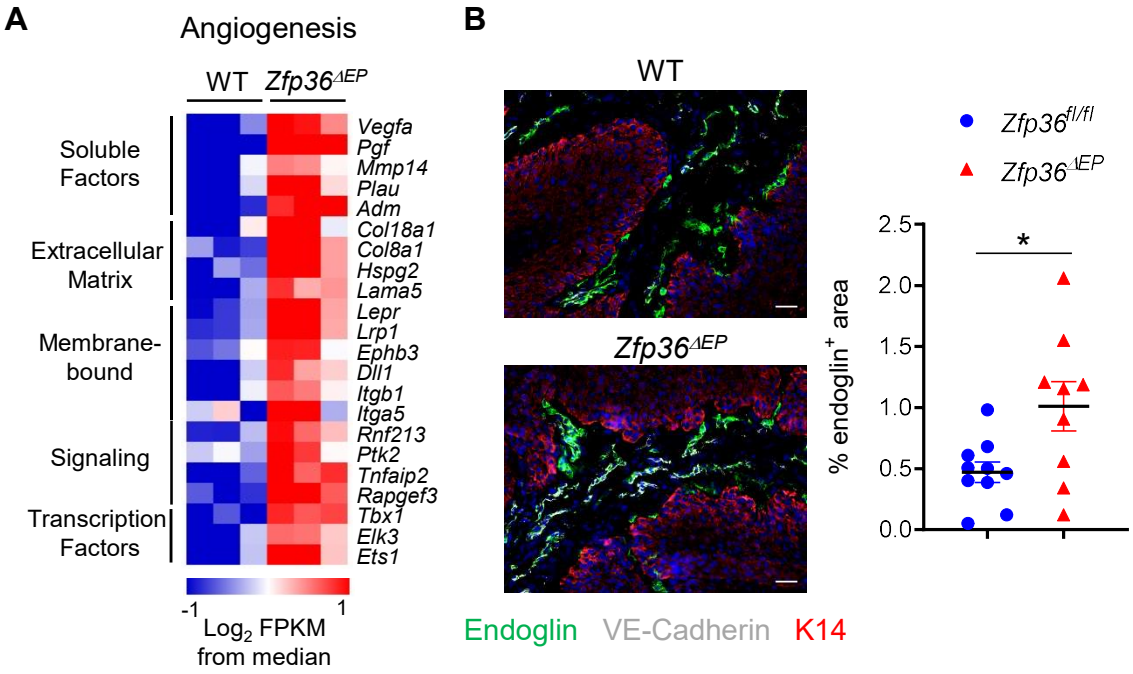

Figure 5: Increased neovascularization of *Zfp36$^{\Delta EP}$* papillomas. (A) Heatmap of expression levels of angiogenesis-related genes significantly increased in *Zfp36*$^{\Delta EP}$ tumor cells in comparison to their WT counterparts. (B) Sections of papillomas (3mm diameter) from *Zfp36$^{\Delta EP}$* and *Zfp36$^{fl/fl}$* mice after 12 weeks of treatment. Cryosections were stained with Endoglin (green), VE-Cadherin (grey), Keratin14 (red) and nuclei (blue). The relative surface of endoglin-positive staining in papilloma sections was measured and graphed (mean ± SEM, n = 9-10). Statistical significance (*$p < 0.05$) was assessed by 2-tailed Mann-Whitney test.

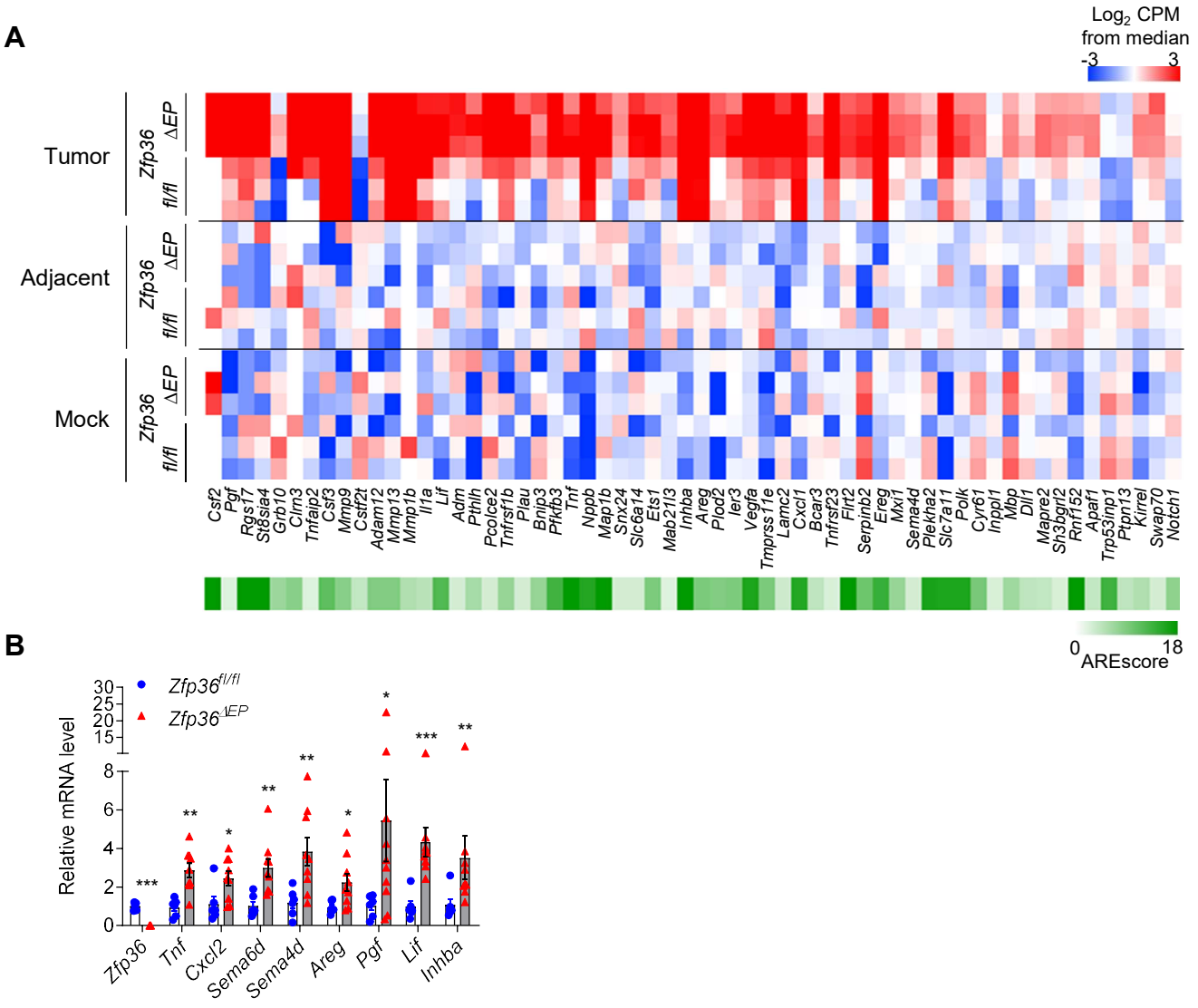

Figure 6: Potential direct targets of TTP in neoplastic epidermal cells. Epithelial cells from tumors, adjacent-treated and mock-treated skin of *Zfp36*$^{\Delta EP}$ and littermates mice were isolated for RNAseq analysis (n = 3). (A) Heatmap of expression levels of transcripts significantly increased or decreased for indicated groups and ARE Score of tumor-specific transcripts from *Zfp36*$^{\Delta EP}$ and *Zfp36*$^{fl/fl}$ samples is shown when >2. (B) mRNA levels of sorted papilloma cells analyzed by qPCR. Levels are normalized against *Actb* and expressed relative to values from the *Zfp36*$^{fl/fl}$ mice, arbitrarily set to 1 (mean ± SEM, n = 7-11, pool of 3 experiments). Statistical significance (**p* < 0.05, ***p* < 0.01, ***p < 0.001) was assessed by 2-tailed Mann-Whitney test.

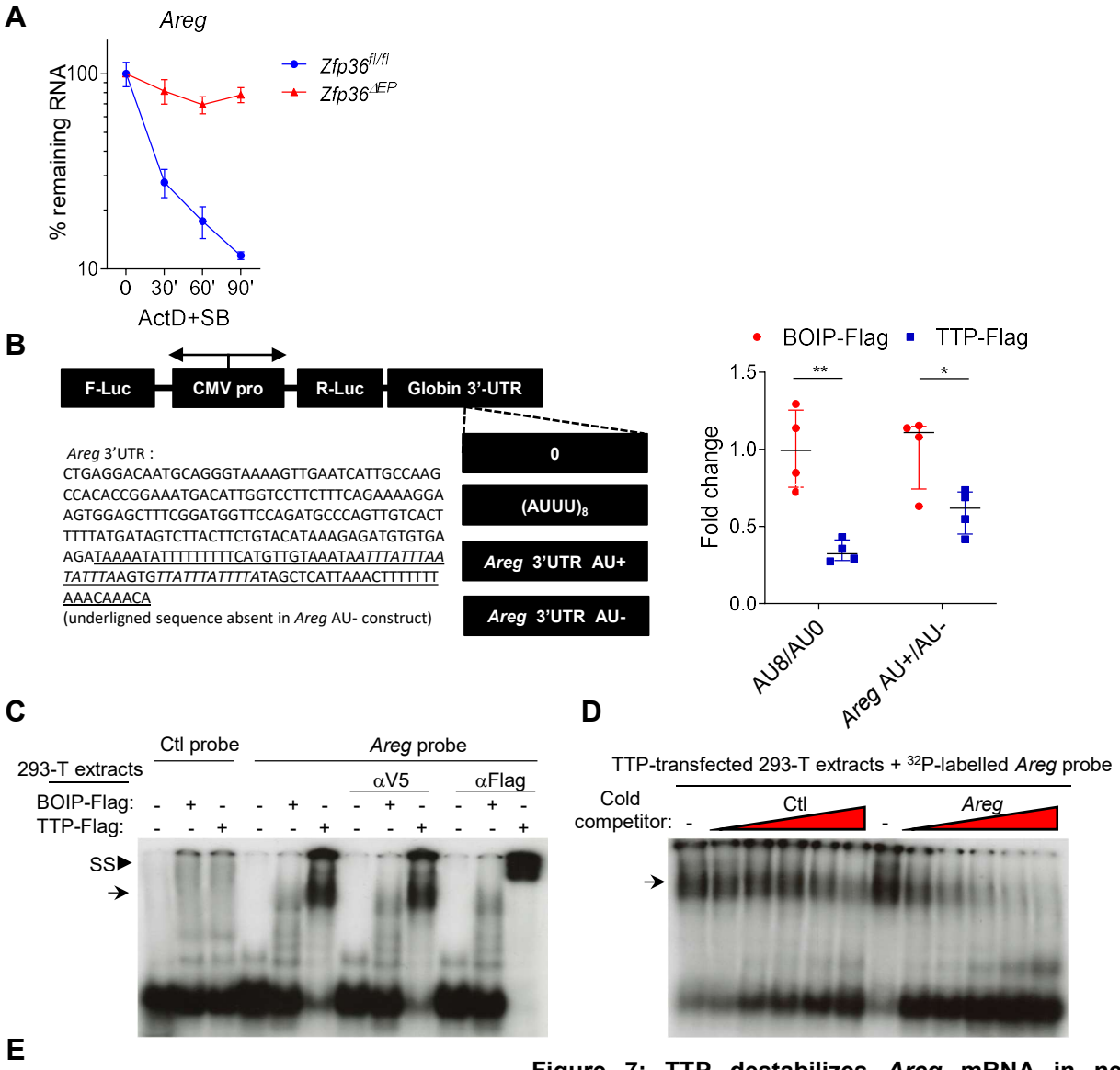

Figure 7: TTP destabilizes *Areg* mRNA in neoplastic epidermal cells. (A) Primary keratinocytes isolated from *Zfp36*$^{fl/fl}$ or *Zfp36*$^{\Delta EP}$ newborns were stimulated with TPA (100 ng/ml) for 2h prior to Actinomycin D (10 µg/µl) and SB202190 (1 µM) treatment for the indicated time Half-life of *Areg* mRNA mRNA was quantified by qPCR and normalized by mRNA levels at t_0 (mean ± SEM, n = 3-4, representative out of 2 experiments). (B) Schematic representation of the dual reporter plasmids generated to assess the role of the ARE elements: 3'UTR of *Areg* mRNA with (AU+) or without (AU-) ARE was inserted behind the sequence coding for *Renilla* luciferase (R-Luc). Fold change between the Rluc/Fluc ratio of AU+ and AU- luciferase signals from dual reporter plasmids co-transfected with TTP-Flag (or BOIP-Flag as control) in HEK293T cells (mean ± SEM, representative out of 7 experiments). (C) Electrophoretic mobility supershift assay. Extracts from HEK293T cells transiently transfected with TTP-Flag or BOIP-flag were incubated with a ^{32}P-labeled probe of *Areg* ARE or a CTRL probe corresponding to pBS polylinker and either no antibody, an α-V5 or an α-Flag antibody before migration.(D) ^{32}P-labeled Areg probe mixed with increasing molar excess of unlabeled Areg probe or pBS control probe was used to performed EMSA competition experiment. (C-D) Results are representative of 3 independent experiments. (E) *Zfp36*$^{\Delta EP}$ mice were treated with DMBA/TPA and 45 min before each application of TPA, mice were treated with the EGFR inhibitor AG1478 (500µg/ml) or vehicle. Mice were monitored for 12 weeks at weekly intervals for tumor development (n = 8-13, representative of 2 experiments). Statistical significance (*p < 0.05, **p < 0.01, ***p < 0.001, ****p < *0.0001*) was assessed by 2-way ANOVA (B) and 2-tailed Mann-Whitney test (E).

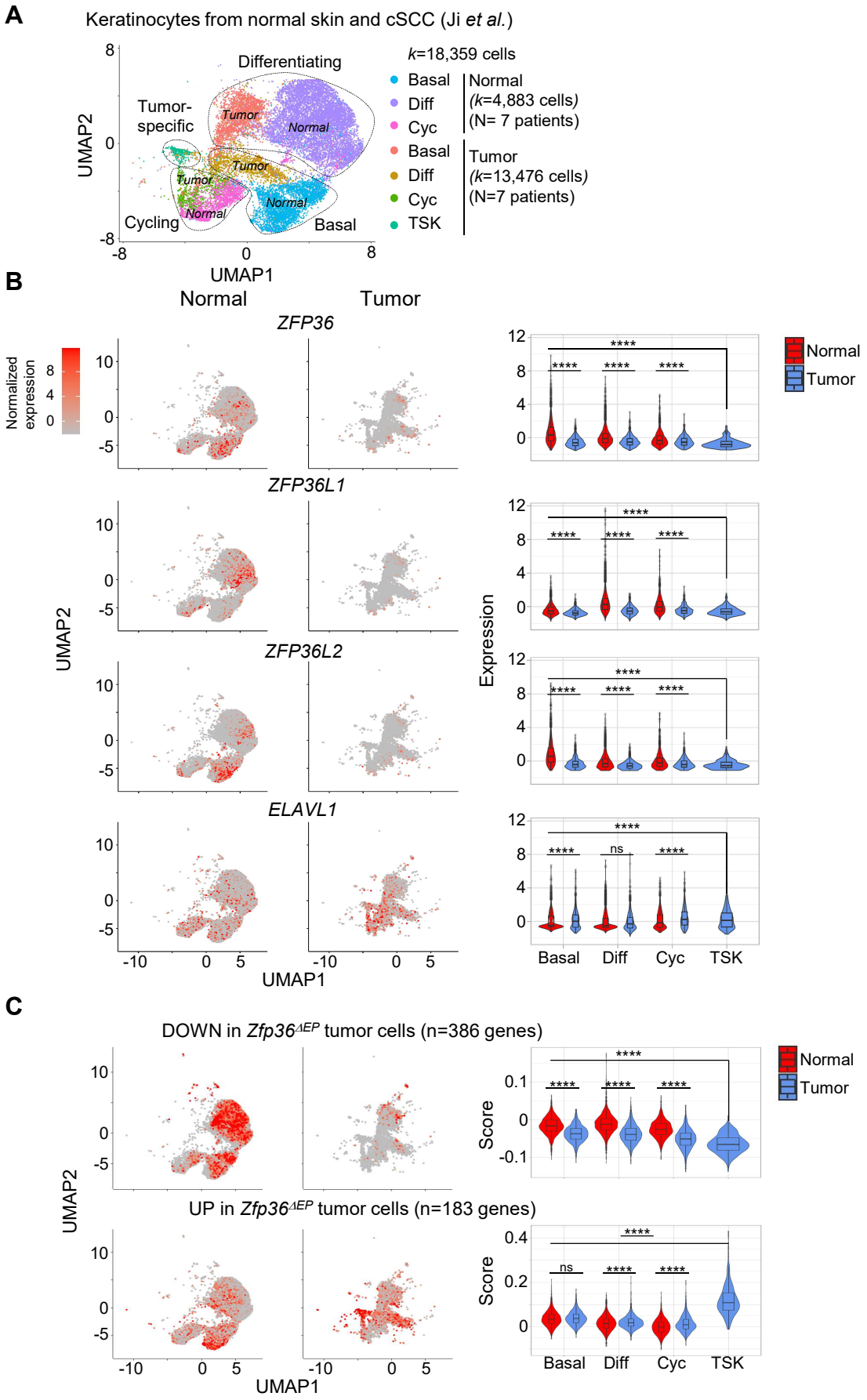

Figure 8: Downregulation of *ZFP36* expression in human tumor-specific keratinocytes. (A) Uniform manifold approximation and projection (UMAP) of 18,359 Single-cell RNA-Seq keratinocytes recovered from the skin of 7 control individuals and from 7 patients with cutaneous squamous cell carcinoma (cSCC) labelled by subsets and origins. (B) Expression of the indicated genes was measured and visualized on UMAP after separating tumor from normal cells or by Violin plots. (C) Enrichment scores of genes that were found to be downregulated (upper panel) or upregulated (lower panel) in *Zfp36*$^{\Delta EP}$ tumor cells visualized on UMAP or by Violin plots. Statistical significance (*$p < 0.05$, **$p < 0.01$, ***p < 0.001, ****$p < 0.0001$) was assessed by 1-way ANOVA with post-hoc Tukey-HSD test.